A multianalysis thermography-based approach for fatigue and damage investigations of ASTM A182 F6NM steel at two stress ratios

Rosa de Finis, Davide Palumbo, Umberto Galietti

▶ To cite this version:

Rosa de Finis, Davide Palumbo, Umberto Galietti. A multianalysis thermography-based approach for fatigue and damage investigations of ASTM A182 F6NM steel at two stress ratios. Fatigue and Fracture of Engineering Materials and Structures, 2018, 42 (1), pp.267-283. ⟨10.1111/ffe.12903⟩. ⟨hal-04725346⟩

HAL Id: hal-04725346

https://hal.science/hal-04725346v1

Submitted on 8 Oct 2024

Received: 16 March 2018 | Revised: 26 June 2018 | Accepted: 14 July 2018
DOI: 10.1111/ffe.12903

ORIGINAL CONTRIBUTION

WILEY

A multianalysis thermography-based approach for fatigue and damage investigations of ASTM A182 F6NM steel at two stress ratios

Rosa De Finis | Davide Palumbo | Umberto Galietti

Department of Mechanics, Mathematics, and Management, Politecnico di Bari, Viale Japigia 182, 70126 Bari, Italy

Correspondence
Rosa De Finis, Politecnico di Bari, Department of Mechanics, Mathematics, and Management, Viale Japigia 182, 70126 Bari, Italy.
Email: rosa.definis@poliba.it

Abstract

Infrared thermography allows an alternative energy-based approach for studying the fatigue behaviour of materials to better understand damage phenomena. In particular, the methodology of infrared thermography can explain the complex dissipative mechanisms promoted by the input parameters, such as the loading ratio, can rapidly provide information about the fatigue strength, and has low cost.

In this work, analysis of the thermographic sequences of ASTM A 182 grade F6NM steel obtained during fatigue testing provided four thermal indexes that were used to investigate the thermoelastic and plastic behaviour of material. Fatigue tests at two opportunely chosen loading ratios ($R = -0.1$, $R = 0.5$) were performed to investigate the relation between the material behaviour and each index at a specific loading ratio. Finally, estimation of the fatigue strength by means of suitable analysis procedures allowed for an investigation of the damage behaviour of materials under specific loading conditions.

KEYWORDS
damage mechanisms, fatigue limit, martensitic steel, stress ratio influence, thermal methods, thermoelastic phase analysis (TPA)

1 | INTRODUCTION

The fatigue behaviour of materials and components is a critical point regarding mechanical characterisation because of the time-consuming tests required and processing of standard procedures, eg, Staircase.[1] Therefore, various techniques and methods have been developed to rapidly and consistently study the various damage phenomena and fatigue behaviours of materials. In this regard, InfraRed Testing (IRT), which is able to provide considerable information on what occurs to the component during the application of a load, can be used to

Nomenclature: b, Parameter related to the linear temperature increase; c_p, Specific heat at a constant pressure [J/kg*K]; E, Young's modulus [MPa]; E_p, Mechanical work executed by the material during the plastic phenomena [J/m^3 cycles]; E_d, Energy per cycle dissipated as heat in the material [J/m^3 cycles]; f, Mechanical loading frequency [Hz]; N, Generic loading cycle; Q, Heat exchanged by convection, conduction, and radiation per cycle [J/m^3 cycles]; R, Stress ratio ($\sigma_{\min}/\sigma_{\max}$); S_d, Thermal signal variations correlated to dissipative processes [signal units]; S_o, Uncalibrated total temperature variations [signal units]; S_{the}, Thermoelastic signal variations [signal units]; T_{in}, Initial temperature offset [°C]; $T_{2\omega}$, Periodic temperature variation two times per loading cycle [°C]; T_{the}, Thermoelastic temperature variations [°C]; T_d, Total temperature [°C]; ψ, Mechanical phase shift between the strain and stress generating hysteresis loops [degree]; φ, Thermoelastic phase shift [degree]; φ_d, Phase shift between the first and second-order temperature components [degree]; ρ, Material density [kg/m^3]; σ_{ij}, Generic component of the stress tensor; ε_{ij}, Generic component of the strain tensor; $\omega = 2\pi f$, Pulsation of the system [rad/s]; ΔT_d, Total temperature variations in a cycle [°C]; ΔU, Internal energy variations [J/cycles] observe many aspects of various physical processes that occur during damage to and failure of materials. The use of thermographic techniques for material characterization allow for contactless investigations and must be considered to be examples of non-stimulated thermography since the analytic procedures consist of observing the natural evolution of the structural behaviour of the component without any external heat sources.[2]

In the literature, a number of researchers have assessed fatigue behaviour by detecting the temperature changes of a material; a number of approaches have been developed.[3-9] Direct temperature measurements have been studied by Luong.[2] The method proposed was based on the linearity of two data series representing the thermal behaviour in both the absence and presence of intrinsic dissipations. The choice of these two data series sometimes results in non-easy evaluations due to the nonlinearity of the data or difficulties in assessing the two behaviours.

In this regard, De Finis[7] based his procedure on the acquisition of a threshold to assess significant temperature variations.

Other approaches are based on energy dissipation measurements.[8-11]

Morabito et al[8] filtered thermoelastic heat sources to assess dissipative heat sources using the numerical models of the heat diffusion equation. However, this approach requires high a computation capacity and long-lasting simulations if the three-dimensional heat diffusion behaviour needs to be investigated. Meneghetti[9] proposed a model for deriving the heat loss per cycle from surface temperature measurements to determine the energy dissipated per cycle.

As reported in a previous work,[7] temperature is affected by different factors (environmental temperature, heat exchanges etc.). Hence, accurate smoothing procedures are required to filter out disturbing heat sources. Moreover, in the presence of low-dissipating materials, such as brittle materials, the heat contribution of the body is very low. Hence, the filtering procedure is essential for data analysis.

Another approach is Thermoelastic Stress Analysis (TSA),[12-21] which is based on an evaluation of the thermoelastic effect[12,13,18-21] under adiabatic conditions. The potentiality of TSA is such that even if the adiabatic conditions are lost, TSA provides the thermoelastic phase shift, a useful tool for localizing and quantifying the damage behaviour of material.[14] The thermoelastic approach is included in a wider approach and involves the analysis of the thermal signal in the frequency domain[19,22-26] to extract the components related to reversible and irreversible temperature variations.

In this approach, however, different assumptions are made regarding temperature variations, but no mention is made about their origin. The intrinsic energy production due to fatigue mechanisms is not taken into account.

It is worth highlighting that the development of irreversible processes in a material is also promoted by specific loading conditions. For example, the influence of the stress ratio[27] is directly related to the strain retardation with respect to the imposed stress. The specific value of the stress ratio, in fact, determines the morphology of the hysteresis loop and, aside from the quantity of heat produced, is correlated to damage. The R-ratio is of great importance in fatigue testing[28-37] and refers to crack formation/propagation at different fatigue regimes (LCF, VHCF etc.) and fracture toughness[38-40] since it is a common opinion that the fatigue strength is reduced as the R-ratio increases.[29,33,34] However, even if the stress ratio is an imposed input parameter that affects the macroscopic behaviour of the material, several studies[41-45] demonstrate how, in the presence of dissipative mechanisms (crack nucleation/initiation/propagation), the stress amplitude conditions locally differ from the imposed conditions due to the incoming plasticization effects.

In the work of Htoo,[41] it is observed that at the notch root, the accumulation of deformation involves a signal inversion of the stress ratio (ie, $R < 0$). This phenomenon is completely governed by plastic phenomena, which also blur any other effects, such as the presence of residual stresses.[44]

An interesting aspect of this topic is that the energy variations produced by irreversible processes determine a second-order temperature effect[24] or thermoelastic phase shift.[21] Hence, it is possible to draw some considerations about the heat dissipated in the material by assessing the temperature signal during the test.

In particular, the aims of the present paper are:

- to study the physical causes of thermal signal variations
- to compare the thermal signal variation at two different loading ratios
- to determine the fatigue behaviour of the steel ASTM A 182 F6NM under two loading conditions: $R = -0.1$ and $R = 0.5$, which were chosen to represent two completely different hysteresis loops by adopting four thermographic indexes

Previous works provide indexes to describe the behaviour of the composites.[46] However, the use of all of the quantities to assess the behaviour of metallic materials at two different loading ratios has not previously been proposed.

Additionally, in previous works,[21-24] the physical aspect of the energy variations that govern the temperature variations was not highlighted, while in this paper, the aim is to explain what produces the heat variations and to correlate these heat changes to temperature changes.

The adopted indexes are:

- the phase shift of the thermoelastic signal (thermoelastic phase analysis—TPA approach[19-21]); "φ," the angle between the temperature signal and stress invariant, which is 0° (or 180°), under adiabatic conditions (the absence of heat exchange between the sample and environment).[16,17] The factors producing heat diffusions in the lattice determine the loss of adiabatic conditions. These factors are the heat produced by the dumping[4,27] of the lattice (negligible at low stress amplitudes), high internal stress gradients related to the imposed load,[21] and local variation of the stress above the yield strength of the material (plastic conditions).[14]
- the amplitude of the second-order temperature signal, "S_d," related to the heat dissipated in the material in the presence of damage[22-24]
- the total temperature signal variations, "ΔS_0," which is strictly related to the mean temperature increase,[2-4] a well-known thermal index for fatigue life evaluations
- the thermoelastic signal "S_{the}" variations correlated with the first stress invariant[18] at the same frequency of the mechanical one

The benefit of using such an approach is that each index can provide a different point of view on fatigue behaviour as each index is related to a specific process. In fact, two different stress ratios (one involving large stress amplitudes and another very close to the yield strength) were chosen for experimental evaluation to shed light on the physical processes that produce dissipative energy variations, which in turn, produce temperature variations.

2 | THEORY

In the absence of material phase transitions, the response of a material to a mechanical cyclic excitation in the presence of dissipative intrinsic processes involves a hysteresis loop due to phenomena producing energy dissipations.[47-49] Considering a cyclic test, in load control, these phenomena determine the retardation of the strain with respect to the imposed stress,[14] here indicated as "ψ" in Figure 1A.

To assess and quantify the energy of the internal friction viscoelasticity and micro-plasticity, one can refer to the dumping phenomena.[27,45] A common procedure involves the study of the area under a generic hysteresis loop.

In Figure 1B, a hysteresis loop is depicted at the most general loading ratio to which all cases can be referred ($R = -1$) in the presence of non-adiabatic deformation process. The figure also reports the completely elastic behaviour of the materials, which is represented by the line k-h. The model of Figure 1B, however, disregards some aspects related to kinematic and isotropic hardening.[47]

Under these conditions, the study of the material behaviour is described by the simple relation between the stress and strain, and the energy of dissipative processes can somehow be quantified by calculating the area of the loop (A_p), which is, in turn, related to the phase shift between the strain and stress, "Ψ."

An important observation results from an analysis of Figure 1B. As the plastic deformations increase two times per loading cycle (one in the loading regime and the second in the unloading regime), the energy involved in this process will always be increasing or almost constant since it is correlated to fatigue heat productions.[50]

Following this, it is possible to state that "$2f$," where "f" is the mechanical frequency of the test, is the fundamental frequency of plastic deformations and then of dissipative phenomena.[23,24]

By focusing our attention on the energy involved in the process, the dissipative phenomena (eg, viscous[45] or plastic phenomena[48]) that occur in the lattice in a fixed finite continuous volume of an isotropic and homogenous material "V_p" can be described using the first principle of thermodynamics:

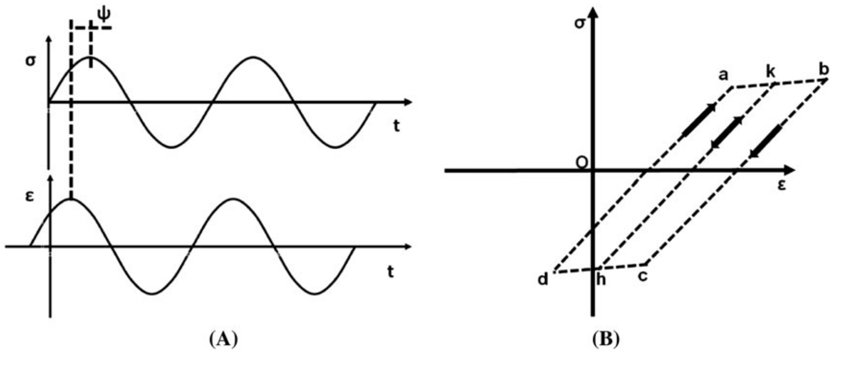

FIGURE 1 Phase shift between strain and stress during (A) fatigue loading and (B) a generic hysteresis loop

$$W_p = \oint \sigma_{ij} d\varepsilon_{ij} \quad (1)$$

where the supplied mechanical energy "W_p" is obtained by integrating the constitutive relation of the material ($\varepsilon_{ij},\sigma_{ij}$).

Equation 1 can be further detailed by separating the different energy contributions present during the fatigue processes[9]:

$$W_p = \Delta U + Q = Q + E_p + E_d \quad (2)$$

where "ΔU" is the internal energy per cycle variation due to the microstructural rearrangements of the persistent slip bands and to all phenomena related to the irreversible dislocation movements in the lattice. A portion of this energy does not remain under mechanical form but is converted into hear. In particular, this energy contributes to the irreversible heat source development in the material and furthermore affects the temperature growth. The term "Q" represents the heat exchanges (radiation, conduction, convection). The term "E_p" refers to the mechanical work introduced in the material system during the plastic phenomena that are a portion of the internal energy "ΔU." "E_d" is the energy per cycle and per unit volume dissipated as heat. E_d includes the irreversible dissipative phenomena related to the viscos-plastic behaviour.

Under the hypothesis:

- most of the dissipated energy is converted to heat
- adiabatic conditions ($Q = 0$) are present
- energy dissipated as heat in the material increases linearly from points "*a*" to "*b*" and "*c*" to "*d*" of the diagram[9,22] shown in Figure 1B

The heat dissipated energy "E_d" in a unit volume of material can be assumed as described by a 2-fold increase in a loading cycle for a fixed stress level, as modelled by De Finis et al.[50] These energy contributions can be determined by the temperature assessment performed during the test. Of course, the temperature will change due to heat generation and the loss of adiabatic conditions, which vary its evolution over time compared with a purely elastic behaviour.

The temperature variations of the material associated with "E_d" will hereafter be indicated as "T_d" while the total temperature variation in one cycle will be referred to as "ΔT_d."

In this way, the energy dissipated per cycle and in a unit of volume of material "E_d" is:

$$E_d = \rho c_p \Delta T_d. \quad (3)$$

The total temperature variation includes all of the temperature variations related to both irreversible and reversible heat dissipations.

In the case of uniaxial stress with sinusoidal loading, the reversible temperature variations can be expressed as follows:

$$T = T_{the} \sin(2\pi\, ft + \pi + \varphi) \quad (4)$$

where "T" are the temperature variations at the mechanical exciting frequency "f," "T_{the}" is the amplitude of the thermoelastic signal, and "φ" is the phase angle between the temperature and loading signal.[21] The symbol "π" has been included according to the classic theory of thermoelastic stress analysis,[14] where the temperature and first stress invariant have opposite signs. Figure 2 depicts the relation between these two quantities under adiabatic conditions (Figure 2A) or not (Figure 2B).

As reported in Figure 2A, the temperature variations and stress in a sample undergoing cyclic loading conditions are generally out-of-phase of a fixed quantity. Apart from this phase shift, the temperature can be delayed by "φ." "φ" depends on several factors. For instance, under linear elastic and adiabatic conditions, its value is zero, but it can change in the presence of phenomena leading to the loss of adiabatic conditions. In Figure 2A, for the finite volume material in the gage length, no heat exchange occurs, so $\varphi = 0$. In Figure 2B, on the other hand, the same volume experiences a dissipative process, which produces a loss of adiabatic conditions. In fact, a phase shift $\varphi \neq 0$ occurs and is summed to π.

In general, the dissipative phenomena may produce heat in the form of two distinct contributions:

- heat produced under hysteresis conditions (viscoelastic regime)[27]
- heat produced under static hysteresis conditions (plastic deformations regime)[51]

In these cases, "φ" varies.

Two opposite cases are useful to explain how different processes contribute to temperature retardation with respect to stress 3.

Under adiabatic conditions, in the case of a perfect linear elastic behaviour, the stress and strain should be in-phase, and "T," the thermoelastic temperature variations, is not-in-phase with "π" (a positive sign of the first stress invariant of Equation 4), [14,17,18] as shown in Figures 2 and 3A.

In Figure 3A, the energy variations related to thermoelastic temperature variations are shown as zeros in a cycle; hence, no temperature increase or accumulation in the material occur.

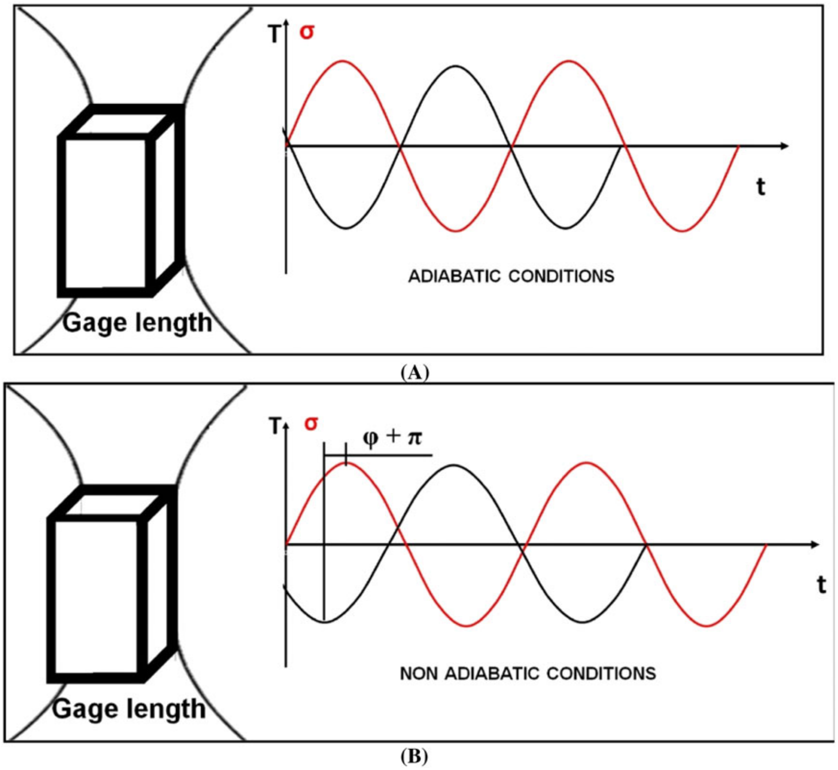

FIGURE 2 Thermoelastic phase shift φ: Temperature and stress relation under adiabatic conditions (A) and under non-adiabatic conditions (B) [Colour figure can be viewed at wileyonlinelibrary.com]

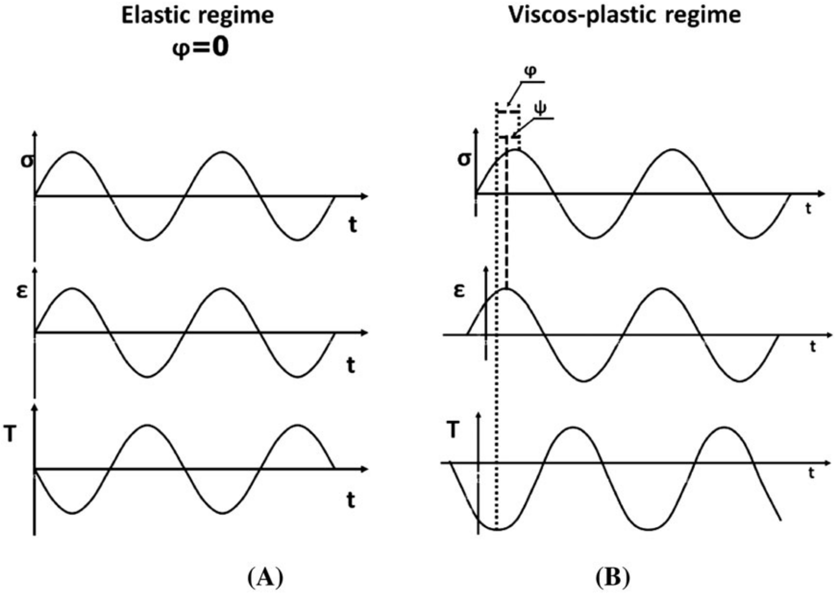

FIGURE 3 Graphical representation of phase shifts between stress–strain and temperature: (A) elastic conditions and (B) viscos-plastic behaviour

Under a viscos-plastic regime, the movements of atoms and local plasticity produce a retardation of the material response to the external excitation, which determines the phase shift between stress and strain, "Ψ," as stated previously[49] (Figure 3B).

Under these conditions, Equation 2 is valid and the intrinsic frictions (reversible and irreversible atoms' movement) that occur in the crystal lattice produce heat.

The heating produced in the lattice leads to a temperature increase and conduction heat exchange so that there is temperature retardation with respect to the imposed stress and the phase shift "φ" assumes a value different from zero.

The quantities "φ" and "Ψ" are strictly related, but here, the aim is to understand the variations of "φ," not to determine each one.

It is important to highlight that the assessment of "φ" also depends on external factors that could affect its measurement, such as a non-perfect homogeneity of the coating, surface scratches, and electronic noise of hardware equipment.

In the following sections, the materials and methods are described, and results are obtained in terms of dissipated heat energy, and the phase signal at two different stress ratios is also discussed.

3 | MATERIAL AND SETUP

The material tested is the low carbon chromium nickel steel ASTM A182 grade F6NM, which is mostly exploited in the gas and oil field due to its high mechanical strength properties and corrosion resistance. The metallurgy of this material is complex: it has a low carbon content associated with the addition of nominally 4% nickel, which allows for the formation of martensitic lath after tempering, resulting in the improvement of its mechanical properties.[51] The weight percent compositions of ASTM A 182 F6NM[52] are reported in Table 1.

TABLE 1 Chemical composition (wt%)

C	Cr	Ni	Mo	S	P	Si	Mn
0.05	11.5-14.00	3.5-5.5	0.5-1.0	0.03	0.03	0.6	0.5-1.0

The material 0.2% proof stress is 617 MPa, the ultimate tensile strength is 755 MPa, and the total elongation is approximately 18%, as listed in the technical guide chart.[52]

The material used in this study was fatigue tested using different procedures. All of the fatigue tests were performed using a servo-hydraulic MTS model 370 loading frame with a capacity of 100 kN.

First, a standard test procedure, the Staircase,[1] was used as a reference test method. Fifteen samples were tested using increasing/decreasing loads according to the failure or success of the sample at two loading ratios, $R = 0.5$ and $R = -0.1$. The test frequency was 39 Hz for both tests, and the loading sequences are reported in Figure 4A, B. The values in terms of the fatigue limit and standard deviation calculated according to the reference[1] were 169.29 MPa (st.dev = 4.44 MPa) for $R = 0.5$ and 250.00 MPa (st.dev =4.52 MPa) for R = −0.1, respectively.

Together with the Staircase campaign, Self-Heating Tests[5] were performed. In this way, "heat sources" were intrinsically produced in the material as the mean stress increased. To set up the loading sequence, which is the sequence of loading blocks (stress semi-amplitudes) imposed on the sample, the yield strength is a good indicator.

Each sequence of loading is composed of 15/20 blocks (the number of cycles is approximately 20 000 per block), each of which is characterised by a constant mean stress, a frequency (17 Hz), and a loading ratio in the manner described by De Finis.[7]

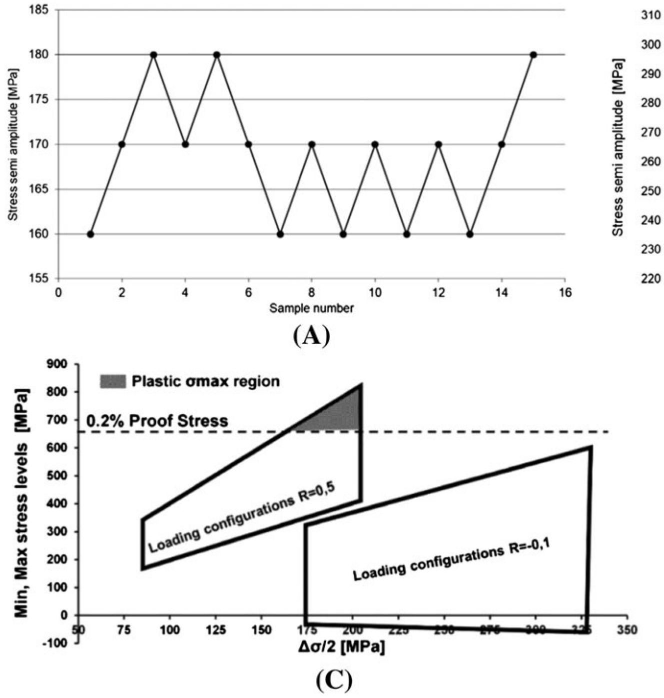

FIGURE 4 Staircase steps, (A) R = 0.5 and (B) R = −0.1; (C) self-heating load configurations at R = 0.5 and R = −0.1; (D) geometry and dimensions of samples

Two different loading configurations were adopted to characterise three samples per loading ratio as reported in Figure 4C. The black edges of the area under the loading configurations in Figure 4C represent the imposed maximum and minimum stresses with respect to the applied stress semi-amplitudes. In Figure 4C, the 0.2% proof stress line is reported, which divides the elastic and plastic regions of loading. At $R = 0.5$, the loading sequence includes more load levels in the plastic regime than that at $R = -0.1$. This condition affects the specific behaviour of the material.

The samples were sized according to the Standard ASTM E 466-96.[53] The relevant dimensions and geometry characteristics are presented in Figure 4D.

The adopted infrared detector Flir X6540 sc (640 × 512 pixels matrix NETD <20 mK) was equipped with a cooled sensor. Three thermal sequences acquired at a frame rate of 100 Hz (1000 frames acquired) for each loading block were acquired after 1000-8000-18 000/20 000 cycles. To increase the efficiency of the measurements, the emissivity of the material surface was increased by applying a thin layer of matte black coating.

4 | METHODS

4.1 | Thermographic signal processing

In Section 2, it is shown that to estimate heat dissipation, it is necessary to detect the surface temperature of the specimen during the test. The temperature variations of the material associated with "E_d " will be hereafter be indicated as "T_d," and the total temperature variation in one cycle will be referred to as "ΔT_d" (Figure 5). In fact, since the linear increase of energy is found to double per cycle, in the material, the temperature variation due to the irreversible processes of fatigue damage will occur at twice the mechanical loading frequency.[22]

Figure 5 shows the temperature variations due to the heat dissipated during a loading cycle in the event that Q = 0. The trend of "T_d" can be decomposed in:

- an offset temperature "T_{in}." The temperature of the body when the cycle starts is supposed to be constant in a loading cycle (this assumption is valid for the duration of the loading step)
- a linear temperature increase over the number of cycles.[8] Its slope is "b"
- a periodic temperature variation (period (1/2)N) with an amplitude "$T_{2\omega}$"

The relation between "ΔT_d" and "$T_{2\omega}$" depicted in Figure 5 is described by Equation 5:

$$\gamma = arctg(T_{2\omega}/(N/4)) = arctg(\Delta T_d/N), \tag{5}$$

then:

$$4T_{2\omega} = \Delta T_d. \tag{6}$$

By assuming that the thermal signal component is a triangular function pulsating at $\omega_0 = 2\omega = 2(2\pi f)$, by expanding it as the sum of cosine function terms, "$T_{2\omega}$" can then be obtained and expanded as

$$\mathrm{T}(t) = \mathrm{T}_{2\omega}/2\ \mathrm{A}\textstyle\sum_1^\infty \left(1/(2\mathrm{n}+1)^2\right)]\cos(2\mathrm{n}\ 1)\omega_0 t), \tag{7}$$

with

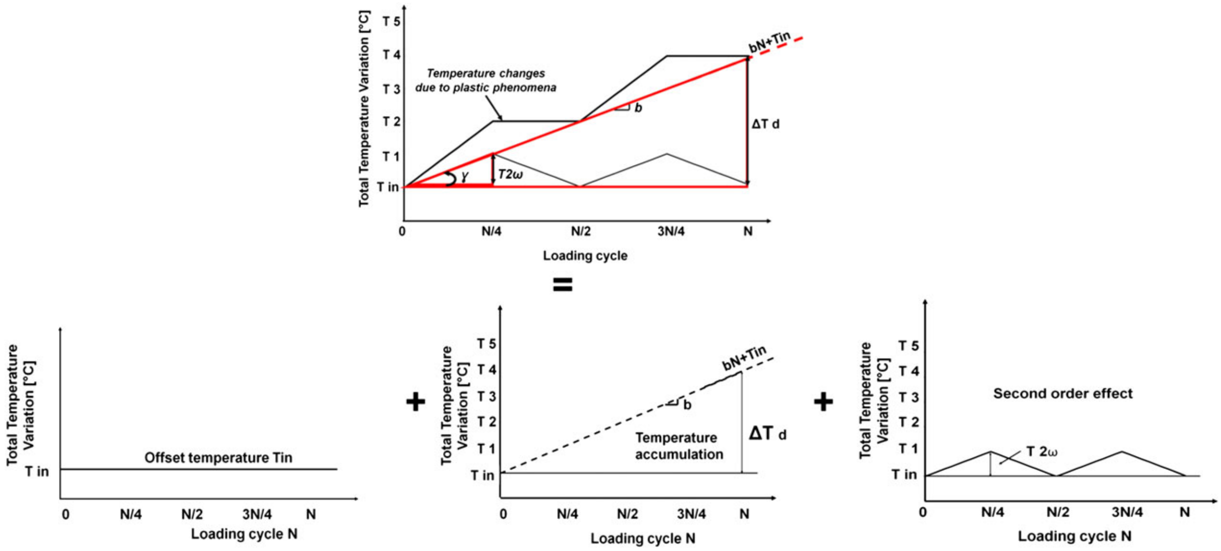

FIGURE 5 Total temperature components and geometric relations between ΔT_d and $T_{2\omega}$ [Colour figure can be viewed at wileyonlinelibrary.com]

$$A = 4T_{2\omega}/9\pi^2. \tag{8}$$

Excluding high order components, for $n = 1$:

$$T(t) = [T_{2\omega}/2]A\cos(2\omega t). \tag{9}$$

Equation 9 shows that it is possible to obtain "ΔT_d" by measuring the thermal signal component that occurs at twice the mechanical frequency, "$T_{2\omega}$." In fact,

$$\Delta T_d = 4T_{2\omega} = 4\left(9\pi^2/4\right)A = 9\pi^2 A. \tag{10}$$

By simply assessing the slope "b" or amplitude "$T_{2\omega}$," the term "E_d" is fully determined.

In general, to obtain the temperature, an output signal acquired by an infrared thermal camera has to be transduced by a suitable calibration to obtain absolute temperature values. Since the focus of this paper is to assess the variations of temperature components and not the absolute temperature, one can operate directly on signal. In this way, the analysis is more rapid, so the temperature signal evolution can be described by

$$S(t) = S_0 + \Delta Sft + S_{the}\sin(\omega t + \pi + \varphi) + A\cos(2\omega t + \varphi_d) \tag{11}$$

where "S" is the uncalibrated thermal signal, and "S_0," "S_{the}," "S_d," *and* "φ" are the four indexes considered in this work to study the fatigue behaviour of a material; "φ_d" is the phase signal of the temperature component at twice the loading frequency. These indexes are related to the mean temperature increase, amplitude of the thermoelastic signal, dissipative sources, and phase of signal "S" at the frequency "f."

All of the thermographic sequences acquired were processed in the IRTA® software, which performs a frequency-domain analysis of the signal to extract the different signal components in terms of four images (data matrix), as shown in Figure 6.

In a few steps, the thermographic indexes were assessed from a single data analysis related to the temperature signal and are expressed in signal units, as shown in Figure 6.

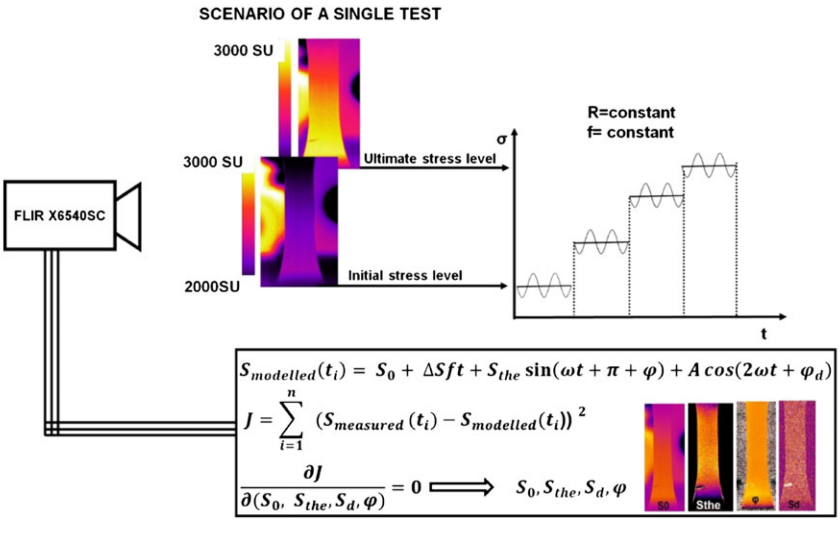

FIGURE 6 From the thermographic signal to the thermal and phase parameters, this figure shows how the IRTA runs [Colour figure can be viewed at wileyonlinelibrary.com]

4.2 | Processing of phase data

The algorithm developed in a Matlab® framework processed the phase data to obtain "$\Delta\varphi$," as represented in Figure 7.The phase matrixes were primarily smoothed using a double-dimension Gaussian kernel. The analysis subsequently required a matrix windowing of the scenario, from $[\varphi]_{MxN}$ to $[\varphi]_{mxn}$, to focus the investigation only on the gauge length of the specimen.

After filtering, since the phase data of the first loading steps[21] are scattered due to the low value of the signal to noise ratio, further processing was required to reduce such an effect. By supposing that the first three loading levels were definitely an elastic regime, where the phase variations were zero, $\Delta\varphi = 0°$, a single mean phase matrix, $[\varphi_m]_{mxn}$, was used in place of the first three steps.

For $R = -0.1$, $[\varphi_m]$ represents the mean matrix value of loading levels 175-190-205 MPa, while at $R = 0.5$, are 85-100-115 MPa. Each value of the matrix is considered to be a non-damaged phase value, and then, all subsequent matrixes can be referred to as this "undamaged condition" by the calculation reported in Equation 12.

$$\left[\Delta\varphi_j\right] = \left[\varphi_j\right] - [\varphi_m] \quad j = 4, \dots\dots\dots N_{last} \tag{12}$$

where "N_{last}" is the last loading level. Consequently, the graphics in Figure 7 start at 220 MPa for data at $R = -0.1$ and at 130 for the data at $R = 0.5$.

From the $[\Delta\varphi_j]$ matrixes, the percentile values 98th and 2nd were extracted, and the difference between

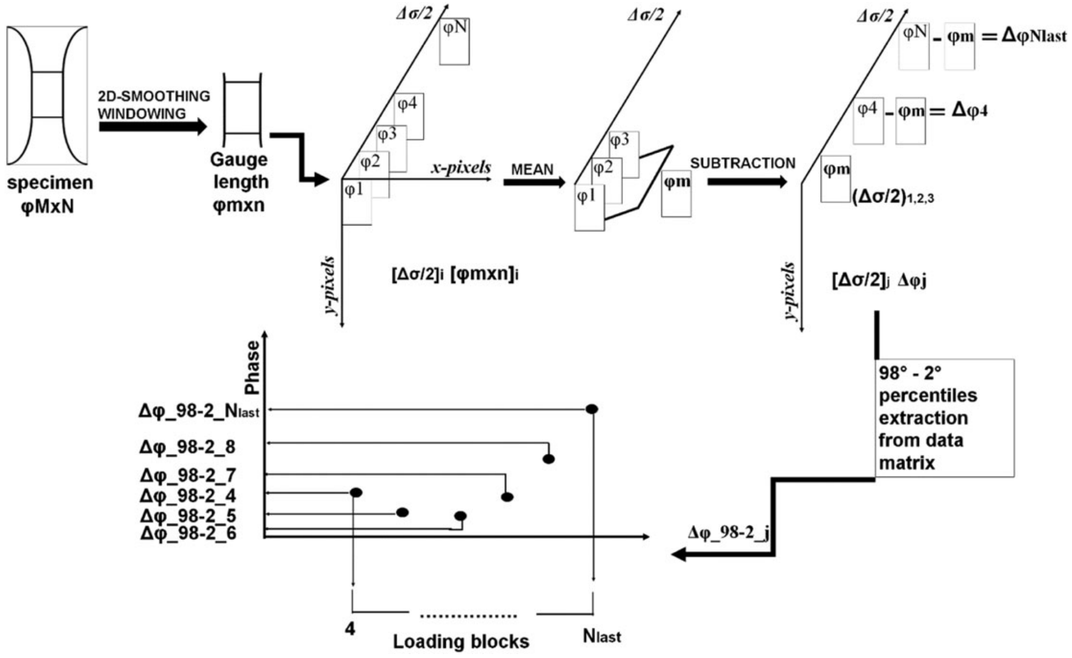

FIGURE 7 Phase data processing procedure: from the 2D map to the phase index

percentiles was calculated to take into account the phase variations. In this way, for a single loading block, the phase parameter used for fatigue limit estimations had a fixed value ($\Delta\varphi_{\_98\text{-}2\_j}$).

The choice of the 98th and 2nd percentiles was made to avoid possible data outliers in the analysis and, at the same time, to refer to values very close to the maximum (or minimum) value of the specific index.

The results for the phase data are presented in Figure 8A for R = −0.1 and Figure 8B for R = 0.5 for three samples.

In Figure 8A,B, the test seemed to be very reproducible since the data scatter was low.

It has been observed that the higher the stress ratio, the higher the phase values: at $R = 0.5$, the phase interval ranged between 1.2° and 2°, while at R = −0.1 the phase variation was approximately 0.3° and 0.6°.

A possible explanation can be due to the stress amplitude effect. At smaller stress amplitudes (higher "*R*"), the hysteresis loop was flattened, and the related plastic phenomena prevailed on viscous phenomena.[54] On the contrary, when the stress amplitude was wider, the viscous phenomena were predominant. In this regard, the phase signal seemed to be a sensitive parameter for describing dissipative phenomena related to plastic stress regime. The material behaves with lower internal dumping,[53] which can explain the different ranges of the variation of "$\Delta\varphi_{\_\ 98\text{-}2perc}$" at different loading ratios.

The procedure continues with the fatigue limit evaluation, as is explained in the following sections.

4.3 | Processing of thermal parameter data

Specific processing procedures of thermal parameters were applied since each parameter represents a specific thermal signal variation.

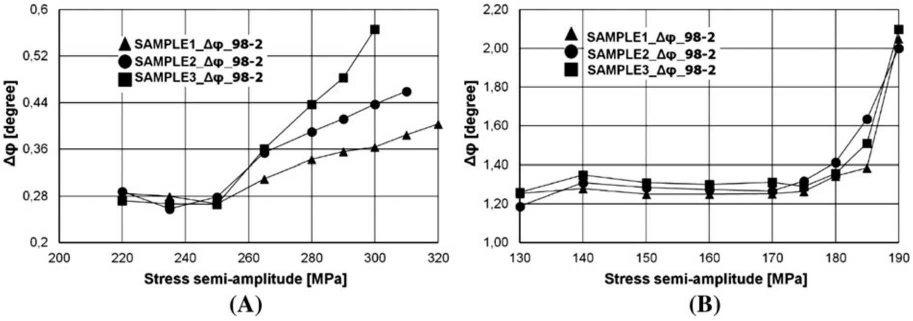

FIGURE 8 Results: Phase data (Δϕ_98-2) at (A) R = −0.1 and (B) R = 0.5

Specifically, for "S_0," heat influence from the environment and the heating from the loading machine grips have to be filtered out, as discussed in De Finis.[7] Furthermore, the value of the 98th percentile was extracted from the matrix, the index ΔS_{0_98}.

The "S_{the}" matrixes (of generic loading block) were also divided pixel by pixel according to the relative stress amplitude ($\Delta\sigma$), and subsequently, the 98th percentile values were extracted from the "S_{the}" matrixes, "S_{the_98}." The temperature changes related to dissipations "S_d" were processed by considering the smoothing and sizing of the matrix to determine "S_{d_98}," which is a thermal parameter related to damage.

All of the operations performed on thermal signal parameters refer to a reduced matrix provided by the windowing of the matrix scenario.

In Figure 9, the output is represented in terms of the "S_{the_98}" curves at $R = -0.1$ (Figure 9A) and $R = 0.5$ (Figure 9B). It is evident that the range of variation of "S_{the}" is the same.

A significant signal increase was obtained before the yield strength for $R = -0.1$, as shown in Figure 9A, and after reaching the yield value for $R = 0.5$, Figure 9B. In fact, as already explained, the thermoelastic signal depended on the stress semi-amplitude. Hence, in the case of R = −0.1, at higher stress values, the signal became nonlinear.

In Figure 10, the results of "S_{d_98}" data are presented, and a different range of variation was detected at two loading ratios even if the behaviour of the whole curves was similar, which means that the tests were perfectly reproducible.

The temperature signal of the intrinsic heat dissipated depended on both plastic and viscous phenomena. When $R < 0$, the higher stress amplitude indicated a wide hysteresis loop area, so that viscous phenomena were able to justify "S_d" values higher than $R > 0$.

At R = 0.5, the energy of plastic phenomena are relatively small, as is the hysteresis loop, with respect to those at $R = -0.1$. "S_d" has small values.

Generally, temperature is a global parameter and is affected by several disturbing heat sources.[2,5,7] By observing the graphs in Figure 11, it is possible to note that the range of the data variation at the two loading ratios is the same. Even if the smoothing procedures are the same for both loading ratios, the noisy characteristic of the curves is more evident at R = −0.1 (Figure 11A) than at R = 0.5 (Figure 11B). Moreover, even for the "ΔS_{0_98}" data, there is not a clear separation in behaviour, specifically at R = −0.1.

However, for all of the curves shown in Figures 9, 10, and 11, the initial sloped trend is more accentuated for temperature signal data at a lower stress ratio (R < 0). This characteristic could be due to the viscous effect produced by the wider stress amplitudes and hysteresis area.

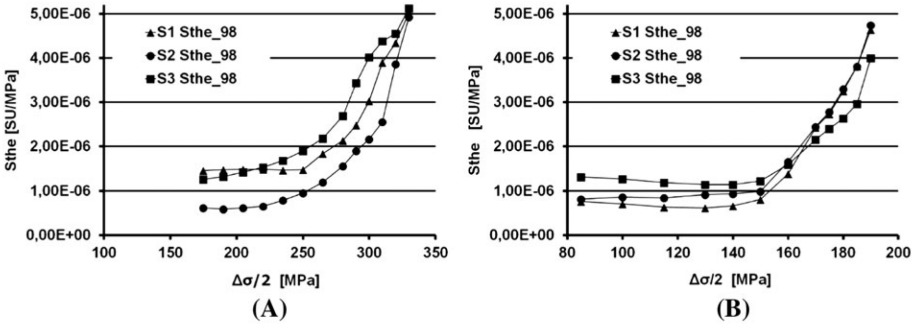

(A) (B)

FIGURE 9 S_{the_98} results at (A) $R = -0.1$ and (B) $R = 0.5$

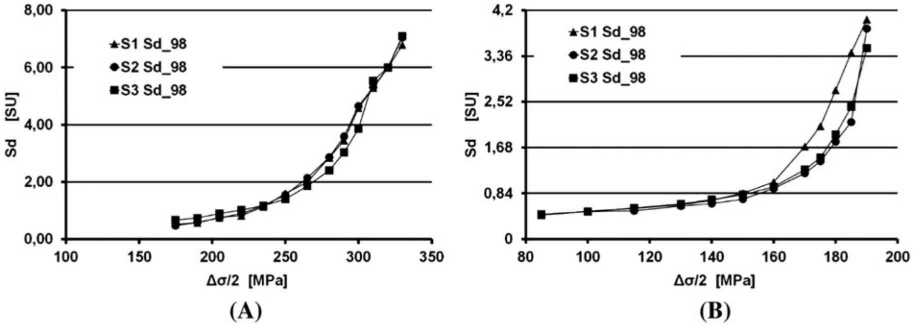

(A) (B)

FIGURE 10 S_{d_98} results at (A) R = −0.1 and (B) R = 0.5

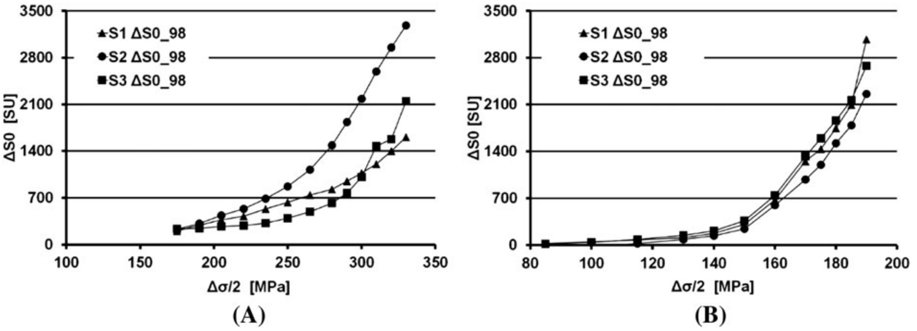

FIGURE 11 ΔS_{0_98} results at (A) R = −0.1 and (B) R = 0.5

4.4 | Influence of the loading ratio on the phase and thermal parameters

In this section, an attempt to explain the influence of the loading ratio on fatigue behaviour is provided by considering the thermal and phase parameter results.

"ΔS_{0_98}" and "S_{the_98}" did not show any remarkable difference within the tests at two loading ratios, while the results of "S_{d_98}" and "$\Delta\varphi_{\_98\text{-}2}$," exhibited a difference depending on the loading ratio that is adopted.

The effect of the stress ratio has also been studied in Fracture Mechanics.[33,55-57] In the work of Kamat,[33] the influence of the stress ratio on the crack closure effect has been demonstrated (crack growth rate "*da/dN*") for a DISPAL aluminium alloy. Other studies[54] have highlighted some differences in the "actual loading ratio" at the crack tip and at a distance from it. However, a higher R means a lower stress amplitude and lower fracture toughness.[58] The influence of "*R*" on fatigue testing was studied on Ti-Al-V alloys for engine turbine blade applications[34] and in a VHCF regime by discussing the relation between "R" and the failure modes. The result was that a high stress ratio played an important role in promoting subsurface micro-cracks.

In an energetic approach,[59] the author addressed the energy stored in the material, which depended on the dislocation arrangement as well as the energy reduction due to clustering and cell formations. The focus of that work was that the quantity of energy stored in the material increased as the loading ratio "*R*" decreased.

This phenomenon opened a wide discussion on the relation between stress ratio and energy involved in the fatigue process, which is represented by the energy of the hysteresis loop. It is likely that the stress ratio can influence the energy contribution within the material since the stress amplitude promotes the type of hysteresis in the material. By considering the Goodman diagram,[54] the higher the stress ratio (lower stress amplitudes), the tighter the hysteresis loop.

It follows that the energy associated with the damage processes that occur in the material is lower than in the case of a material undergoing fatigue testing at lower stress ratios (higher stress amplitudes); moreover, the energy associated with the damage processes depends on the specific dissipative process activated in the material.[49]

Under the hysteresis regime, in which both components exist, one can predominate over others depending on the stress ratio. In particular, at a stress ratio close to one, the test runs very close to the mechanical static properties of materials, such as the yield strength; the plastic phenomena may be more probable than other viscous phenomena.[36] The latter occur at lower stress ratios, where the hysteresis loop is wider and the intrinsic frictions are at grain scale.

The "$\Delta\varphi_{\_98\text{-}2}$" data are higher at $R = 0.5$ than at $R = -0.1$, possibly due to the dominating plastic effects on the hysteresis loop. It seems that the phase data are more influenced by the plasticity than the dumping properties.

At lower stress ratios, the viscous phenomena are enhanced[29] due to the wider characteristic of the hysteresis loop. The "S_{d_98}" results, on the contrary, exhibit higher values at $R = -0.1$ than at $R = 0.5$. A possible explanation for this phenomenon can be attributed to the size of the hysteresis loop, which determines the major energy dissipated during fatigue processes in the material.

5 | RESULTS

5.1 | Fatigue limit estimation

5.1.1 | Phase parameter $\Delta\varphi_{\_98\text{–}2}$

The assessment of the fatigue limit by analysing the phase data involves a specific data analysis algorithm. The calculations assume that the fatigue limit is "the point of the series, from which the signal prevails over the noise". Following this, a slope analysis was performed to determine the point of the slope change, which is the first positive value of the series ($\Delta\varphi$ threshold is 0°).

The method has already been successfully adopted on phase data of composite materials in the work of Palumbo.[46]

For the sake of simplicity, the results are shown quantitatively in Table 1 and graphically in Figure 12.

In Table 2, data series “$\Delta\varphi_{\_98\text{-}2}$” at R = 0.5 and R = −0.1 are reported for each sub-step, as are the mean value and slope calculations for sample 1.

The criterion adopted was to consider as a fatigue limit the first value above the 0° threshold, so that for sample 1 at R = 0.5, it is 160 MPa, while for the test running at R = −0.1, it is 250 MPa.

Figure 12A,B reports a comparison of “$Slope\_\Delta\varphi_{\_98\text{-}2}$” at R = 0.5 and R = −0.1, respectively. At $R > 0$, there is low scatter and good reproducibility between the curves, while the results at R = −0.1 appear to be affected by noise, especially at higher stress semi-amplitudes. However, the data that are significant for the evaluation of the fatigue limit are those occurring at lower stress amplitudes.

5.1.2 | Thermal parameters: ΔS_0, S_{the}, S_d

Thermal parameters were processed for evaluating the fatigue limit using a method described in the work of De Finis[7] of the series “ΔS_{0_98},” “S_{the_98},” and “S_{d_98}.”

The procedure is based on residual assessment ($\Delta S_{0\_98\_residuals}$, $S_{the\_98\_residuals}$, $S_{d\_98\_residuals}$) from the series “ΔS_{0_98},” “S_{the_98},” and “S_{d_98}.” Finally, a threshold is calculated to determine the fatigue limit.

The first points of the series “$\Delta S_{0\_98\_residuals}$,” “$S_{the\_98\_residuals}$,” and “$S_{d\_98\_residuals}$” that exhibit values higher than the values of the threshold is the fatigue limit estimation.

The global results are shown in Table 3 along with the results of the reference tests that were carried out. The assessed fatigue limit at $R = 0.5$ generally underestimates the value obtained by the reference test method (particularly for “ΔS_0”). In fact, the error related to the application of the threshold method on ΔS_0 is 13%. However, a more accurate evaluation can be achieved by reducing

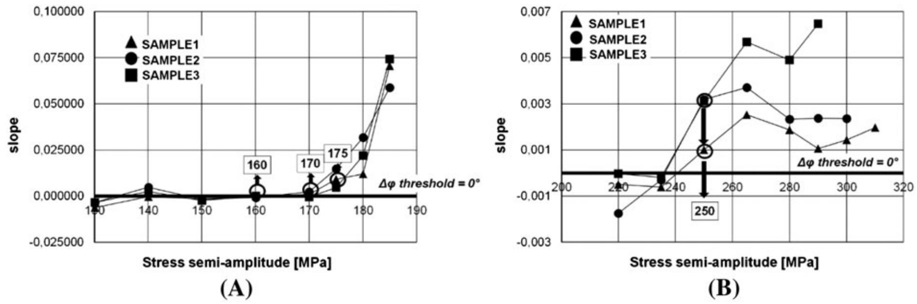

(A) (B)

FIGURE 12 Phase data and slope results for each specimen at (A) $R = 0.5$ and (B) R = −0.1

TABLE 2 Data series of $\Delta\varphi_{\_98-2}$, for fatigue limit estimation of sample 1

	***R* = 0.5**						***R* = −0.1**				
	$\Delta\varphi_{\_98\text{-}2}$ [°]						**$\Delta\varphi_{\_98\text{-}2}$ [°]**				
Δσ/2 [MPa]	**Sub-step1**	**Sub-step2**	**Sub-step3**	**Mean**	**Slope $\Delta\varphi_{\_98\text{-}2}$**	**Δσ/2 [MPa]**	**Sub-step1**	**Sub-step2**	**Sub-step3**	**Mean**	**Slope $\Delta\varphi_{\_98\text{-}2}$**
85	2.58	2.63	2.55	2.59		175	0.31	0.32	0.33	0.32	
100	1.7	1.67	1.62	1.66	−0.03881	190	0.29	0.29	0.32	0.3	−0.00086
115	1.41	1.41	1.46	1.43	−0.01362	205	0.28	0.29	0.31	0.29	−0.00052
130	1.27	1.26	1.23	1.25	−0.00629	220	0.27	0.28	0.3	0.28	−0.00050
140	1.27	1.27	1.29	1.28	−0.00022	235	0.27	0.27	0.29	0.28	−0.00061
150	1.24	1.26	1.25	1.25	−0.00146	250	0.26	0.26	0.28	0.27	0.00100
160	1.22	1.27	1.26	1.25	0.00012	265	0.29	0.31	0.33	0.31	0.00254
170	1.24	1.25	1.27	1.25	0.00089	280	0.35	0.33	0.35	0.34	0.00188
175	1.27	1.26	1.26	1.26	0.00914	290	0.36	0.34	0.37	0.36	0.00106
180	1.33	1.37	1.33	1.34	0.01195	300	0.36	0.35	0.38	0.36	0.00144
185	1.34	1.42	1.39	1.38	0.07056	310	0.38	0.38	0.4	0.38	0.00197
190	1.99	2.07	2.09	2.05		320	0.4	0.39	0.43	0.4	

TABLE 3 Fatigue limit estimations using phase data and thermal parameters data at two loading ratios

a
Loading ratio $R = 0.5$
Values in MPa

Sample	1	2	3	Avg	Std. dev.	%error
$\Delta\varphi$	160.00	170.00	175.00	168.33	7.64	−0.63%
ΔS_0	140.00	150.00	150.00	146.67	5.77	+13.00%
$\mathbf{S}_{\mathrm{the}}$	150.00	160.00	150.00	153.33	5.77	+ 9.49%
Sd	150.00	160.00	140.00	150.00	10.00	+11.45%
	Staircase fatigue limit reference			169.40	4.38	

b
Loading ratio R = −0.1
Values in MPa

Sample	1	2	3	Avg	Std. dev.	%error
$\Delta\varphi$	250.00	250.00	250.00	250.00	0.00	0.00%
ΔS_0	265.00	250.00	250.00	255.00	8.66	+2.00%
$\mathbf{S}_{\mathrm{the}}$	265.00	235.00	250.00	250.00	15.00	0.00%
Sd	235.00	235.00	250.00	240.00	8.66	−4.00%
	Staircase fatigue limit reference			250.00	4.77	

the “distance” between each loading block. “$\Delta\varphi$” seems to be the only value that provides a fatigue limit that is very close to the Staircase reference. In fact, the percentage error is only 0.63% in absolute value. However, all of the values reported in Table 3a tend to be lower than the reference value, so one can state that the procedure provides almost conservative results.

The results for the tests running at $R < 0$ in Table 3b are closer to those of the fatigue limit Staircase reference. The percentage error in comparison to the Staircase reference is very low for all indexes. In particular, in this case, “ΔS_0” slightly overestimates the reference value, while “S_d” provides an underestimation of the fatigue limit with the same data scatter (standard deviation 8.66 MPa). Even in this case, “$\Delta\varphi$” is capable of accurately determining a fatigue limit very close to the reference in the same way as “S_{the}.” In fact, the percentage error is null in referring to “S_{the},” and the data dispersion is higher.

5.2 | Damage analysis: Parameter maps

In this section, the capability of “φ,” “S_{the},” and “S_d” for damage analysis of a material is shown. Graphical analysis is a useful tool for localising and determining the region of dissipative phenomena and failures.

For the first sample of each loading ratio, “φ,” “S_{the},” and “S_d” maps are presented to observe the onset of damage in the material and to provide a possible explanation for referring to the specific damage mechanism associated with the loading ratio regime. Figures 13, 14 depict the maps for three stress semi-amplitude levels, before, after, and at the estimated fatigue limit: 140/165/180 MPa (test at $R = 0.5$) and 220/250/300 MPa (tests at $R = -0.1$), respectively.

In Figure 13A,B,C, respectively, the “φ,” “S_{the},” and “S_d” maps exhibit the onset of the damage process in correspondence with the stress level of the estimated fatigue limit (approximately at 165 MPa). The region of interest as well as the dimension seems to be similar. To better observe these processes, a profile contouring operation (two levels) was performed with Matlab® software. This analysis sheds light on the effective dimension of the damaged regions. In particular, the areas detected in phase maps and “S_{the}” coincide with less than the sign, which is opposite, while “S_d” seems to include the regions represented by “φ” and “S_{the}.” However, the results slightly depend on the number of the contouring level chosen.

In Figure 13D, for the specific loading level above the fatigue limit (180 MPa), whole profiles were superimposed into a single map (called *ALL*), demonstrating that the areas belong to the same region all of the parameters provide single information on the damage. The potential of the technique clearly involves the joint use of the maps to detect the onset of the dissipative mechanism.

Nevertheless, by comparing three images, it is possible, even qualitatively, to detect the region of damage at

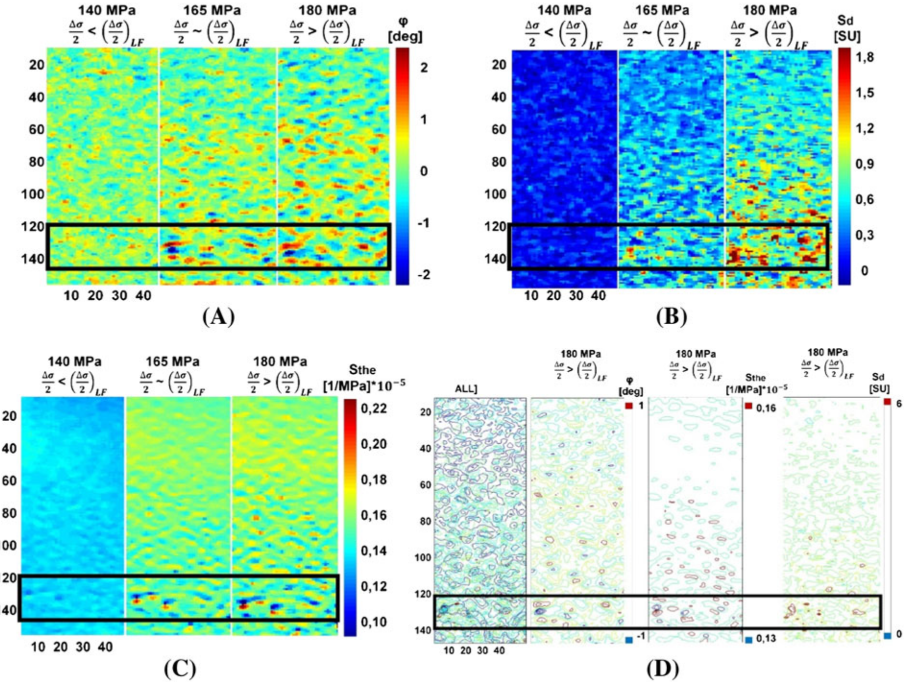

FIGURE 13 Damage analysis of sample 1 tested at $R = 0.5$ (A) phase, (B) S_d, (C) S_{the}, and (D) contouring of all of the parameter maps [Colour figure can be viewed at wileyonlinelibrary.com]

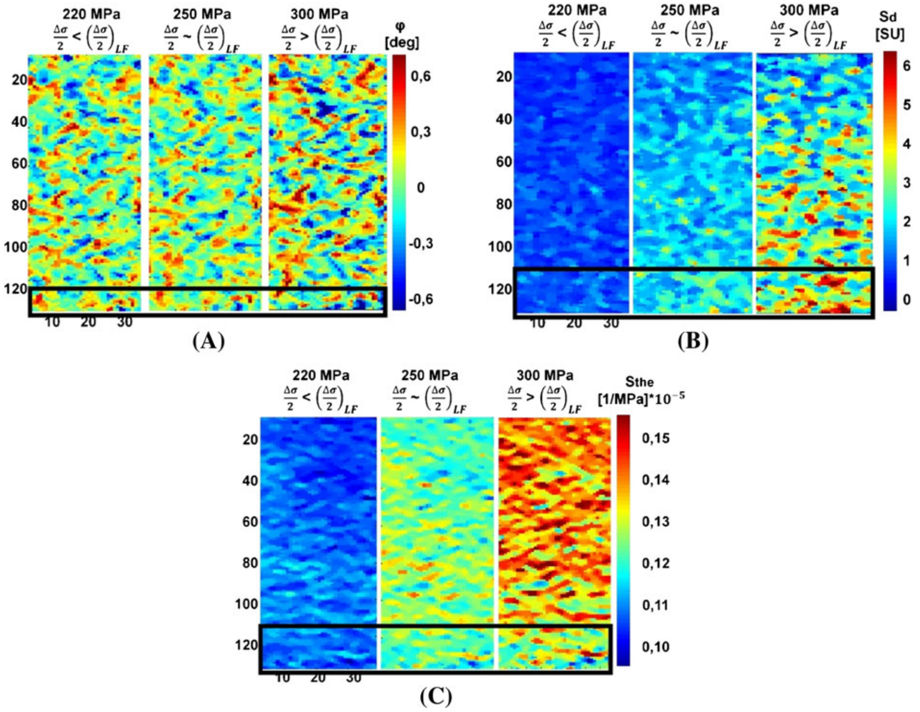

FIGURE 14 Damage analysis of sample 1, tested at $R = -0.1$, (A) phase; (B) S_d; (C) S_{the} [Colour figure can be viewed at wileyonlinelibrary.com]

the early stages. The specimen failed in the zone in the black squared region.

At $R < 0$, in Figure 14A, no predominant effect of damage is present, but widespread positive/negative clusters are detectable in the matrix. A global phase signal increase is recorded from below to above-fatigue-limit stress blocks.

In Figure 14B, "S_d" exhibits a global increasing signal from 220 to 300 MPa. In effect, high maximum values of the signal are evident at the stress level above the fatigue limit (300 MPa). This effect affects the downward part of the "S_d" map and is characterised by large clusters. In the phase and "S_d" maps, attention can be focused on the zone enclosed by a black line, which is the region of failure where the dissipative phenomena seem to be concentrated.

The "S_{the}" signal at $R = -0.1$ in Figure 14C presents a signal increase in the central part of the gauge length. A localised process is detected at the bottom right side of the matrix, starting at 250 MPa. Even for three parameters evaluated at R = −0.1, it is possible to correlate the zone of the dissipative phenomena with the proximity of a crack process.

As represented by the maps in Figures 13, 14, the dissipative phenomena are different depending on the loading ratio. At $R = 0.5$, the contrast between damaged/undamaged zones is higher than at $R = -0.1$. In particular, at $R = 0.5$, the onset of a crack is easily detectable in Figure 13A-D, and the plastic component is predominant.

On the contrary, at $R = -0.1$, where the viscous component prevails (Figure 14), the dissipative phenomena are widespread in the gauge length. "S_{the}" seems to be more accurate for detecting the onset of a crack with respect to the phase maps. "S_d" maps at R = −0.1 present a viscos-plastic zone, mostly in the area represented by the black box. The fact that there is no localised damage could be due to the viscous behaviour, which prevails over the plastic one.

6 | CONCLUSIONS

In this paper, six samples of ASTM A182 F6NM martensitic steel were fatigue tested using the well-known "self-heating" procedure with the aims of:

- comparing the thermal signal variation at two completely different loading ratios ($R = -0.1$ and $R = 0.5$)
- providing a mechanical characterisation of the material

The analysis in the frequency domain of the thermal signal provided different parameters (Δφ ΔS0, Sthe, Sd), which represent both the thermoelastic and dissipative effects.

The goals of the present research were to provide:

- a more in-depth understanding of proposed indexes, where "Δφ" seems to be more influenced by plastic than the viscos-plastic behaviour, while "Sd" is related to the energy of intrinsic dissipations in the material and "Sthe" allows the detection of crack initiation
- the possibility of reducing the time of an experimental campaign. When the threshold is assessed, theoretically, it is not mandatory to run the test until sample failure.
- online characterisation of the damage
- a fatigue limit estimation that was in good agreement with the Staircase method at two different loading ratios.

ACKNOWLEDGEMENTS

This work is part of a large-scale research project (PON-SMATI) aimed at identifying innovative steels for use of turbomachinery under extreme environmental conditions. The authors would like to thank GE Oil & Gas (Nuovo Pignone S.r.l.) for the support and collaboration they provided during the experimental tests.

ORCID

Rosa De Finis http://orcid.org/0000-0002-7972-345X

REFERENCES

1. UNI 3964. Prove meccaniche dei materiali metallici, Prove di fatica a temperatura ambiente, Principi generali, 1985.
2. Luong MP. Infrared thermographic scanning of fatigue in metals. *Nucl Eng Des*. 1995;158(2-3):363-373.
3. Luong MP. Infrared observation of thermomechanical couplings in solids. Thermosense XXIV conference, part of SPIE's Aerosense, 1-5 April 2002, Orlando (Florida)
4. Yang B, Liaw PK, Morrison M, et al. Temperature evolution during fatigue damage. *Intermetallics*. 2005;13(3-4):419-428.
5. La Rosa G, Risitano A. Thermographic methodology for the rapid determination of the fatigue limit of materials and mechanical components. *Int J Fatigue*. 2000;22(1):65-73.
6. Fargione G, Geraci A, La Rosa G, Risitano A. Rapid determination of the fatigue curve by the thermographic method. *Int J Fatigue*. 2001;24:11-19.
7. De Finis R, Palumbo D, Ancona F, Galietti U. Fatigue limit evaluation of various martensitic stainless steels with new robust thermographic data analysis. *Int J Fatigue*. 2015;74:88-96.
8. Morabito AE, Chrysochoos A, Dattoma V, Galietti U. Analysis of heat sources accompanying the fatigue of 2024 T3 aluminium alloys. *Int J Fatigue*. 2007;29(5):977-984.
9. Meneghetti G. Analysis of the fatigue strength of a stainless steel based on the energy dissipation. *Int J Fatigue*. 2007;29(1):81-94.
10. Boulanger T, Chrysochoos A, Mabru C, Galtier C. Calorimetric analysis of dissipative and thermoelastic effects associated with the fatigue behavior of steels. *Int J Fatigue*. 2006;26:221-229.
11. Chrysochoos A, Huon V, Jourdan F, Muracciole JM, Peyroux R, Wattrisse B. Use of full-field digital image correlation and

infrared thermography measurements for the thermomechanical analysis of material behaviour. *Strain*. 2010;46(1):117-130.

12. Medgenberg J, Ummenhofer T. Assessment of fatigue damage in low-carbon steel using lock-in-thermography. 8th international conference of Quantitative Infrared Thermography (QIRT), June 28-30 2006, Padova (Italy)
13. Palumbo D, Galietti U. Data correction for thermoelastic stress analysis on titanium components. *Experimental Mechanics*. 2015;56(3):451-462. https://doi.org/10.1007/s11340-015-0115-0
14. Harwood N, Cummings WM. *Thermoelastic Stress Analysis*. Bristol: Adam Hilger; 1991.
15. Dunn SA. Using nonlinearities for improved stress analysis by thermoelastic techniques. *Appl Mech Rev*. 1997;50(9):499-513.
16. Stanley P. Beginnings and early development of thermoelastic stress analysis. *Strain*. 2008;44(4):285-287.
17. Pittaresi G, Patterson EA. A review of the general theory of thermoelastic stress analysis. *J Strain Analysis*. 1999;35:35-39.
18. Wang WJ, Dulieu-Barton JM, Li Q. Assessment of non-adiabatic behaviour in thermoelastic stress analysis of small scale components. *Exp Mech*. 2010;50(4):449-461.
19. Palumbo D, Galietti U. Characterization of steel welded joints by infrared thermographic methods. *Quantitative Infrared Thermography Journal*. 11(1):29-42.
20. Ancona F, Palumbo D, De Finis R, Demelio GP, Galietti U. Automatic procedure for evaluating the Paris law of martensitic and austenitic stainless steels by means of thermal methods. *Eng Fract Mech*. 2016;163:206-219.
21. Palumbo D, Galietti U. Thermoelastic phase analysis (TPA): a new method for fatigue behaviour analysis of steels: TPA: a new method for fatigue behaviour analysis of steels. *Fatigue Fract Eng Mater Struct*. 2016;40(4):523-534. https://doi.org/10.1111/ffe.12511
22. Enke NF, Sandor BI. Cyclic plasticity analysis by differential infrared thermography. *Proceeding of the VII International Congress on Experimental Mechanics*. 1988;830-835.
23. Sakagami T, Kubo S, Tamura E, Nishimura T. Identification of plastic-zone based on double frequency lock-in thermographic temperature measurement. International conference of fracture ICF11 2015, Catania (Italy)
24. Krapez JK, Pacou D, Gardette G. Lock-in thermography and fatigue limit of metals. Quantitative infrared thermography, QIRT, 18-21 July 2000. *Reims (France)*.
25. Kim KS, Jung HC, Akhter N, Chang HS, Kim MK, Kim DS, Jung DW. Thermoelastic stress analysis of a fatigue specimen using the lock-in infrared thermography. 7th International Conference on NDE in Relation to Structural Integrity for Nuclear and Pressurized Components, 12-15 May 2009, Yokohama (Japan)
26. Galietti U, Palumbo D, De Finis R, Ancona F. Fatigue damage evaluation with new thermal methods. 3rd International Workshop on Advanced Infrared Technology and Applications, September 11-14 2013, Tourin (Italy)
27. Audenino AL, Crupi V, Zanetti EM. Correlation between thermography and internal damping in metals. *Int J Fatigue*. 2003;25(4):343-351.
28. Mayer H, Schuller R, Karr U, et al. Mean stress sensitivity and crack initiation mechanisms of spring steel for torsional and axial VHCF loading. *Int J Fatigue*. 2016;93:309-317.
29. Surajit KP. Numerical models of plastic zones and associated deformations for elliptical inclusions in remote elastic loading-unloading with different R-ratios. *Eng Fract Mech*. 2016;152:72-80.
30. Sakai T, Sato Y, Nagano Y, Takeda M, Oguma N. Effect of stress ratio on long life fatigue behavior of high carbon chromium bearing steel under axial loading. *Int J Fatigue*. 2016;28: 1547-1554.
31. Mayer H, Schuller R, Karr U, et al. Cyclic torsion very high cycle fatigue of VDSiCr spring steel at different load ratios. *Int J Fatigue*. 2015;70:322-327.
32. Ishihara S, McEvily AJ, Sato M, Taniguchi K, Goshima T. The effect of load ratio on fatigue life and crack propagation behavior of an extruded magnesium alloy. *Int J Fatigue*. 2009;31(11-12):1788-1794.
33. Kamat SV, Srinivas M. Effect of load ratio on the fatigue crack growth behaviour of DISPAL 2 alloy. *Int J Fatigue*. 1999;21(2):169-172.
34. Yang K, He C, Huang Q, et al. Very high cycle fatigue behaviors of a turbine engine blade alloy at various stress ratios. *Int J Fatigue*. 2017;99:35-43.
35. Karadag M, Stephens RI. The influence of high R ratio on unnotched fatigue behavior of 1045 steel with three different heat treatments. *Int J Fatigue*. 2003;25(3):191-200.
36. Müller T, Sander M. Investigation of variable amplitude loading and stress ratio in the very high cycle fatigue regime using micro-notched specimens. *Proc Eng*. 2015;101:322-329.
37. Kovacs S, Beck T, Singheiser L. Influence of mean stresses on fatigue life and damage of a turbine blade steel in the VHCF-regime. *Int J Fatigue*. 2013;49:90-99.
38. Pannemaecker A, Fouvry S, Brochu M, Buffiere JY. Identification of the fatigue stress intensity factor threshold for different load ratios R: from fretting fatigue to C (T) fatigue experiments. *Int J Fatigue*. 2016;82:211-225.
39. Zhu ML, Xuan FZ, Tu ST. Effect of load ratio on fatigue crack growth in the near-threshold regime: a literature review, and a combined crack closure and driving force approach. *Eng Fract Mech*. 2015;141:57-77.
40. Toribio J, Matos JC, González B. Micro- and macro-approach to the fatigue crack growth in progressively drawn pearlitic steels at different R-ratios. *Int J Fatigue*. 2009;31(11-12):2014-2021.
41. Htoo AT, Miyashita Y, Otsuka Y, Mutoh Y, Sakurai S. Variation of local stress ratio and its effect on notch fatigue behaviour of 2024-T4 aluminum alloy. *Int J Fatigue*. 2016;88:19-28.
42. Knop M, Jones R, Molent L, Wang C. On the Glinka and Neuber methods for calculating notch tip strains under cyclic load spectra. *Int J Fatigue*. 2000;22(9):743-755.
43. Kumar Paul S, Stanford N, Taylor A, Hilditch T. The effect of low cycle fatigue, ratcheting and mean stress relaxation on

stress-strain response and microstructural development in a dual phase steel. *Int J Fatigue*. 2015;80:341-348.

44. Gaur V, Doquet V, Persent E, Mareau C, Roguet E, Kittel J. Surface versus internal fatigue crack initiation in steel: influence of mean stress. *Int J Fatigue*. 2016;82:437-448V.
45. Mortezavi V, Haghshenas A, Khonsari MM, Bollen B. Fatigue analysis of metals using damping parameter. *Int J Fatigue*. 2016;91:124-135.
46. Palumbo D, De Finis R, Demelio GP, Galietti U. Study of the damage evolution in composite materials based on the thermoelastic phase analysis (TPA) method. *Composite Part B*. 2016;17:49-60.
47. Akazawa T, Nakashima M, Sakaguchi O. Simple model for simulating hysteretic behaviour involving significant strain hardening. WCEE Eleventh World Conference on Earthquake Engineering 1996. ISBN: 0080428223.
48. Polák J, Petrenec M, Kruml T, Chlupová A. Cyclic plastic response and fatigue life in symmetric and asymmetric cyclic loading. *Proc Eng*. 2011;10:568-577.
49. Maquin F, Pierron F. Heat dissipation measurements in low stress cyclic loading of metallic materials: from internal friction to micro-plasticity. *Mech Mater*. 2009;41(8):928-942.
50. De Finis R, Palumbo D, Silva MM, Galietti U. Is the temperature plateau of a self-heating test a robust parameter to investigate the fatigue limit of steels with thermography? *Fatigue Fract Eng Mater Struct*. 2017 https://doi.org/10.1111/ffe.12738;41(4):917-934.
51. Giannozzi M, Baldassarre L, Cecconi M, et al. About design, materials selection and manufacturing technologies of centrifugal compressors for extreme sour and acid service. ADIPEC Technical Conference 10-13 November 2013. *Abu Dhabi (UAE)*.
52. Technical guide tachart: http://www.tachart.com/material/astm-a182-f6nm/
53. ASTM E 466–96. Standard practice for conducting force controlled constant amplitude axial fatigue tests of metallic materials 2002.
54. Juvinall R, Marshek K. *Fundamental of Machine Component Design*. ETS: John Wiley & Sons Inc; 1994.
55. De Finis R, Palumbo D, Galietti U. Mechanical behaviour of stainless steels under dynamic loading: an investigation with thermal methods. *Journal of Imaging*. 2016;2(4):2(4). https://doi.org/10.3390/jimaging2040032
56. Kujawski D. Enhanced model of partial crack closure for correlation of R-ratio effects in aluminum alloys. *Int J Fatigue*. 2001;23(2):95-102.
57. Zhang J, He XD, Du SY. A simple engineering approach in the prediction of the effect of stress ratio on fatigue threshold. *Int J Fatigue*. 2003;25(9-11):935-938.
58. Warren J, Wei DY. A microscopic stored energy approach to generalize fatigue life stress ratios. *Int J Fatigue*. 2010;32(11):1853-1861.
59. Frunză G, Diaconescu EN. Hysteresis and mechanical fatigue. The annals of university “dunărea de jos” of galaţi fascicle VIII, Tribology 61–66 2006, issn 1221-4590.

How to cite this article: De Finis R, Palumbo D, Galietti U. A multianalysis thermography-based approach for fatigue and damage investigations of ASTM A182 F6NM steel at two stress ratios. *Fatigue Fract Eng Mater Struct*. 2018;1–17. https://doi.org/10.1111/ffe.12903